imaging (fig. S5) (*18*) that intermediate and small particles are retained in the catalyst after the 98-hour aging treatment. Hence, the beneficial effect of the acid pretreatment is not short lived. We consider that with appropriate development and reaction engineering (i.e., scaling up using continuous flow reactors with pelleted or extruded catalyst formulations), our discovery, made using powdered catalysts in a small-scale batch autoclave reactor, can underpin the generation of H_2O_2 at the 3 to 8% concentration levels required in most chemical and medical applications

One benefit of the direct process (*24*) is that it will permit local synthesis on a small scale as and when required, thereby ensuring that H_2O_2 no longer needs to be stored or transported, both of which are potentially hazardous, as demonstrated by a recent road tanker explosion in the United Kingdom (*25*). In particular, the process lends itself to small-scale generation of H_2O_2, which could be of great value for the production of medical antiseptics where the H_2 would be generated from water by electrolysis.

References and Notes

1. H. T. Hess *et al.*, Eds., *Kirk-Othmer Encyclopedia of Chemical Engineering* (Wiley, New York, 1995).
2. J. Van Weynbergh, J. P. Schoebrechts, J. C. Colery, U.S. Patent 5447706, (1992).
3. J. H. Lunsford, *J. Catal.* **216**, 455 (2003).
4. D. P. Dissanayake, J. H. Lunsford, *J. Catal.* **206**, 173 (2002).
5. D. P. Dissanayake, J. H. Lunsford, *J. Catal.* **214**, 113 (2003).
6. V. R. Choudhary *et al.*, *Chem. Commun. (Camb.)* **2004**, 2054 (2004).
7. P. Landon *et al.*, *Phys. Chem. Chem. Phys.* **5**, 1917 (2003).
8. J. K. Edwards *et al.*, *J. Mater. Chem.* **15**, 4595 (2005).
9. M. J. Maraschino, U.S. Patent 5169618 (1992).
10. V. R. Choudhary, C. Samanta, *J. Catal.* **238**, 28 (2006).
11. V. R. Choudhary, P. Jana, *J. Catal.* **246**, 434 (2007).
12. V. R. Choudhary *et al.*, *Appl. Catal.* **317**, 234 (2007).
13. J. K. Edwards *et al.*, *Catal. Today* **122**, 397 (2007).
14. B. E. Solsona *et al.*, *Chem. Mater.* **18**, 2689 (2006).
15. J. K. Edwards *et al.*, *Faraday Discuss.* **138**, 225 (2008).
16. J. K. Edwards *et al.*, *J. Catal.* **236**, 69 (2005).
17. J. K. Edwards *et al.*, *Green Chem.* **10**, 388 (2008).
18. Materials and methods are available as supporting material on *Science* Online.
19. A. A. Herzing *et al.*, *Faraday Discuss.* **138**, 337 (2008).
20. Q. Liu *et al.*, *Angew. Chem. Int. Ed.* **47**, 6221 (2008).
21. M. Turner *et al.*, *Nature* **454**, 981 (2008).
22. A. A. Herzing *et al.*, *Science* **321**, 1331 (2008).
23. M. Chen *et al.*, *Science* **310**, 291 (2005).
24. *The Chemical Engineer* **766**, 16 (2005).
25. BBC News, 30 August 2005; http://news.bbc.co.uk/1/hi/england/london/4197500.stm

26. Supported by the Engineering and Physical Sciences Research Council of the United Kingdom and Johnson Matthey PLC (project ATHENA) and the European Union (project AURICAT, HPRN-CT-2002-00174). C.J.K. and A.A.H. are funded by: NSF DMR-0079996, NSF DMR-0304738, and NSF-DMR-0320906. A.A.H. thanks the NRC for support through the postdoctoral associate program. We thank A. Roberts and C. Blomfield (Kratos Analytical) for assistance with XPS measurements, and P. Collier, P. Ellis, and P. Johnston (Johnson Matthey) for discussions on analysis, provision of ICP analysis data, and design of the sequential experiments.

Supporting Online Material

www.sciencemag.org/cgi/content/full/323/5917/1037/DC1
Materials and Methods
SOM Text
Figs. S1 to S5
Table S1

25 November 2008; accepted 9 January 2009
10.1126/science.1168980

Strong Release of Methane on Mars in Northern Summer 2003

Michael J. Mumma,[1]* Geronimo L. Villanueva,[2,3] Robert E. Novak,[4] Tilak Hewagama,[3,5] Boncho P. Bonev,[2,3] Michael A. DiSanti,[3] Avi M. Mandell,[3] Michael D. Smith[3]

Living systems produce more than 90% of Earth's atmospheric methane; the balance is of geochemical origin. On Mars, methane could be a signature of either origin. Using high-dispersion infrared spectrometers at three ground-based telescopes, we measured methane and water vapor simultaneously on Mars over several longitude intervals in northern early and late summer in 2003 and near the vernal equinox in 2006. When present, methane occurred in extended plumes, and the maxima of latitudinal profiles imply that the methane was released from discrete regions. In northern midsummer, the principal plume contained ~19,000 metric tons of methane, and the estimated source strength (≥0.6 kilogram per second) was comparable to that of the massive hydrocarbon seep at Coal Oil Point in Santa Barbara, California.

The atmosphere of Mars is strongly oxidized, composed primarily of carbon dioxide (CO_2, 95.3%), along with minor nitrogen (N_2, 2.7%), carbon monoxide (CO, 0.07%), oxygen (O_2, 0.13%), water vapor (H_2O, 0 to 300 parts per million), and radiogenic argon (1.6%); other species and reduced gases such as methane (CH_4) are rare. CH_4 production by atmospheric chemistry is negligible, and its lifetime against removal by photochemistry is estimated to be several hundred years (*1*–*3*) or shorter if strong oxidants such as peroxides are present in the surface or on airborne dust grains (*4*). Thus, the presence of substantial amounts of CH_4 would require its recent release from subsurface reservoirs; the ultimate origin of this CH_4 is uncertain, but it could be either abiotic or biotic (*2*, *5*, *6*).

Before 2003, all searches for CH_4 were negative (*7*–*9*). Since then, three groups have reported detections of CH_4 (*10*–*18*); see (*19*–*24*) for discussion. Spectral data from the Mars Express mission contain five unidentified spectral features between 3000 and 3030 cm^{-1}, one of which coincides with the expected position of the CH_4 Q branch (*15*, *18*, *25*). The data span all seasons and extend over several years, but low S/N ratios require averaging the spectra over two of the three key dimensions (longitude, latitude, and time). Other searches featured low spatial coverage (*16*) or sparse seasonal coverage (*16*, *17*), and the results (CH_4 mixing ratios) are best interpreted as upper limits.

We report measurements of CH_4 in northern summer in 2003 and estimate its source strength and its (short) destruction lifetime. Our search covered about 90% of the planet's surface and spanned 3 Mars years (MYs) (7 Earth years). Our results (*10*–*14*) are based on the simultaneous detection of multiple spectrally resolved lines of CH_4, and each observation is spatially resolved, allowing examination of spatial and temporal effects. Our spatial maps reveal local sources and seasonal variations.

To search for CH_4 and other gases on Mars, we used the high-dispersion infrared spectrometers at three ground-based telescopes. Here we report data from CSHELL/IRTF (Hawaii) and NIRSPEC/Keck-2 (Hawaii) [supporting online material text 1 (SOM-1)]. Each spectrometer features a long entrance slit that is held to the central meridian of Mars (Fig. 1A) while spectra are taken sequentially in time (fig. S1). Pixelated spectra were acquired simultaneously at contiguous positions along the entire slit length, for each observation, providing 35 spectra at 0.2–arc second (arc sec) intervals (~195 km at disk center) when Mars' diameter is 7 arc sec (Fig. 1A). We binned these data (in groups of three along the slit) to provide latitudinally resolved spectra, and then in time (longitude) to improve the S/N ratio (SOM-1). Here we focus on three dates in 2003 [universal time (UT) 12 January, 19 March, and 20 March] and one in 2006 (UT 26 February) (Table 1).

Our spectra exhibit strong lines of terrestrial H_2O ($2\nu_2$ band) and CH_4 (ν_3) along with weaker lines of O_3 ($3\nu_3$) seen against the continuum (Fig. 1, B and C, top). We corrected the data for telluric extinction (SOM-2). At 3.3 μm, Mars is seen mainly in reflected sunlight, so the collected spectra also contain Fraunhofer lines (SOM-3). Removing these two components from a composite spectrum exposed the residual Mars atmospheric spectrum (Fig. 1, B and C) (*26*). One line of CH_4 and three distinct lines of H_2O are seen in each panel.

CH_4 consists of three separate nuclear spin species (A, E, and F) that act as independent

[1]NASA Goddard Space Flight Center, Mailstop 690.3, Greenbelt, MD 20771, USA. [2]Department of Physics, Catholic University of America, Washington, DC 20008, USA. [3]NASA Goddard Space Flight Center, Mailstop 693, Greenbelt, MD 20771, USA. [4]Department of Physics, Iona College, New Rochelle, NY 10801, USA. [5]Department of Astronomy, University of Maryland, College Park, MD 20742–2421, USA.

*To whom correspondence should be addressed. E-mail: michael.j.mumma@nasa.gov

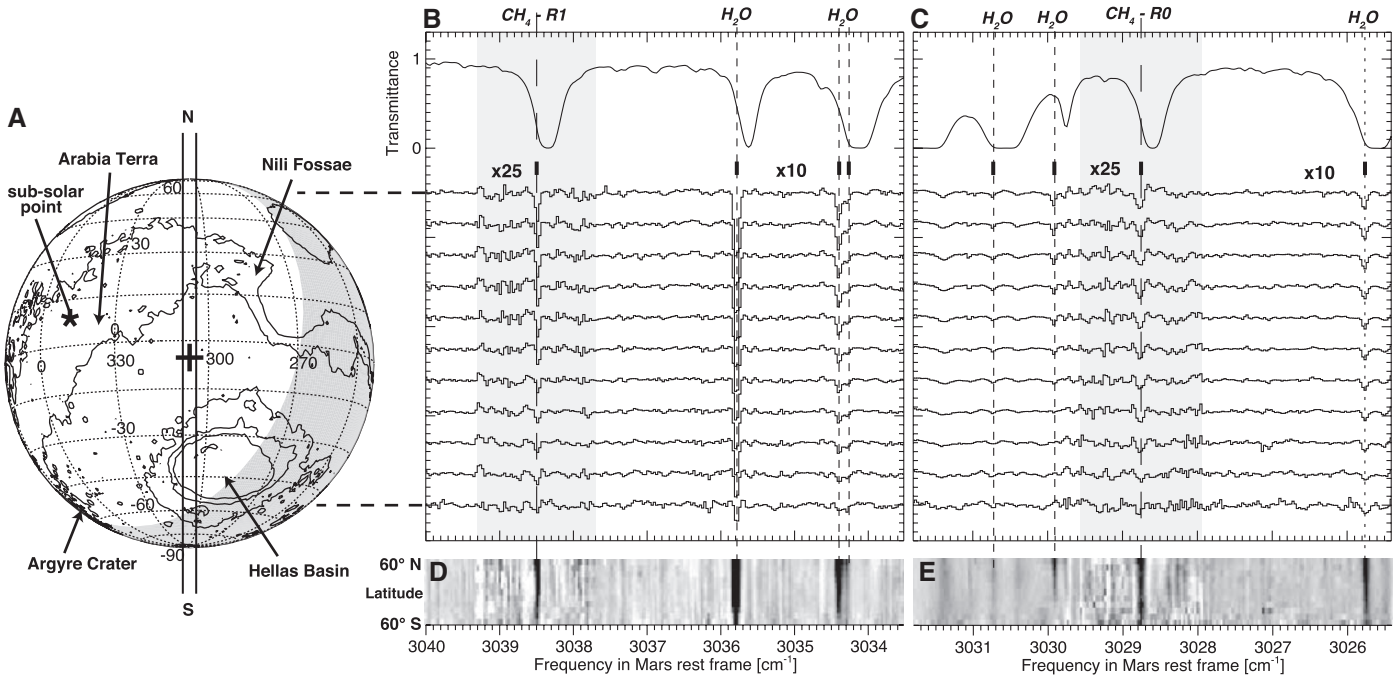


Fig. 1. Detections of CH_4 and water vapor on Mars on UT 19 and 20 March 2003. (**A**) Mars is shown as it appeared at the mean time of the R0 and R1 observations (Table 1). The subsolar (*) and sub-Earth (+) points are marked, along with several prominent features. Contours of constant altitude are shown at intervals of 3 km, and regions beyond the afternoon terminator (the night side) appear in gray. The entrance slit of the spectrometer was oriented north-south (N-S) on Mars along the central meridian and is shown to scale. (**B**) Spectra taken on 20 March were extracted at 11 equal intervals (0.6 arc sec each) along the slit (ranging from 70°N to 70°S), after binning over longitudes 277° to 323°W. At the sub-Earth position, the binned spectrum samples a footprint 3215 km (east-west) by 586 km (N-S) (see text and SOM-1). Strong lines of terrestrial water and CH_4 (labeled) and weak lines of ozone (3036 to 3038 cm^{-1}) appear in a typical spectrum, shown at the top of this panel. See SOM-3 for data reduction. Narrow spectral lines of H_2O (three lines, short dashes) and CH_4 (the R1 line, long dashes) are seen at the Doppler-shifted positions expected for this date. Corresponding Mars ozone (O_3) absorptions for this date are weak and would appear in the southern polar region (not sampled). (**C**) Spectra taken on 19 March are shown as in (B) but binned over the longitude range from 289° to 335°. Spectral lines of H_2O (three lines, short dashes) and CH_4 (the R0 line, long dashes) are seen. The longitude range sampled was systematically westward (by 12°) of that sampled for R1 (Table 1), owing to the slower rotation of Mars relative to Earth. The residual spectra shown in (B) and (C) are scaled by a factor of either 10 or 25 (gray background), to make the lines more apparent. (**D** and **E**) show residual intensities in a grayscale format, to more easily show the spatial distribution of the gases with latitude. The lines are displayed as measured; that is, corrections for two-way air mass on Mars (Sun to Mars surface and Mars surface to Earth), for Mars local topography, and for terrestrial transmittance have not yet been applied to the residuals (see Fig. 2).

spectral entities. The identification of two spectrally resolved CH_4 lines (R0 and R1, of the A and F species, respectively) and the good agreement (within measurement error) of the CH_4 column densities obtained independently from each line support our detection (systematic uncertainty and stochastic errors are discussed in SOM-2 and SOM-3). At a later season [areocentric longitude of the Sun (L_s) = 220°], we detected the P2 doublet, consisting of lines of the E and F species (SOM-1 and fig. S2). Detections (or upper limits) reported by others are based on the intensity summed over the frequencies of multiple unresolved lines [the Q branch (*15*, *18*)] or on the summed intensity of several undetected individual lines (*16*, *17*).

Column densities and mixing ratios for CH_4 obtained from the spectra of Fig. 1 show a broad CH_4 plume in late summer when averaged over 46° in longitude (Fig. 2, A and B) (SOM-3); more restricted longitudinal binning shows higher maxima (Fig. 2C, profile d). In early spring (profile a), the CH_4 mixing ratio was small at all latitudes and showed only a hint of the marked maximum seen in late summer. By early summer (profiles b and c), CH_4 was prominent but the maximum mixing ratio occurred at more northerly latitudes and was somewhat smaller than in late summer. The late summer profile (d) in Fig. 2C differs from the profile shown in Fig. 2B, owing to different longitudinal binning (*27*). The mixing ratios shown in Fig. 2C (profile d) represent a subset of the data of Fig. 1B, centered at central meridian longitude (CML) 310° (see aspect, Fig. 1A) and binned over only 30 min. Including the slit width, 30-min binning provides a footprint at the sub-Earth point that spans ~16° (948 km) in longitude and 10° (586 km) in latitude (fig. S1 and Table 1).

A quantitative release rate can be inferred by considering the observed temporal changes (with season) and measured spatial profiles. The summer mixing ratios (profiles b, c, and d) show a

Table 1. Observational searches for Mars CH_4 on selected dates. A complete listing of all dates searched, spanning 7 years, is available from the authors.

Date and observation range (UT)	Mars season (L_s, °)	Longitude range (CML, °)	Doppler shift (km s^{-1})	CH_4 line searched	Footprint* (°longitude by °latitude)
2003 – MY 26					
11 January 19:36–20:34	121.5	274–288	–14.7	R1	22° × 14°
12 January 17:20–20:18	121.9	231–274	–15.0	R1	22° × 14°
13 January 17:05–20:07	122.4	218–262	–15.0	R0	22° × 14°
19 March 15:41–18:50	154.5	289–335	–15.7	R0	16° × 10°
20 March 15:34–18:44	155.0	277–323	–15.6	R1	16° × 10°
2006 – MY 27 to 28					
16 January 04:49–07:03†	357.3	303–336	+16.1	R0, R1	
26 February 01:28–02:53	17.2	223–244	+17.1	R1	13° × 10°

*Centered on the sub-Earth point, binned over 30 min in time and 0.6 arc sec along the slit. †Using NIRSPEC/Keck-2 (SOM-3); all other listed observations used CSHELL/IRTF.

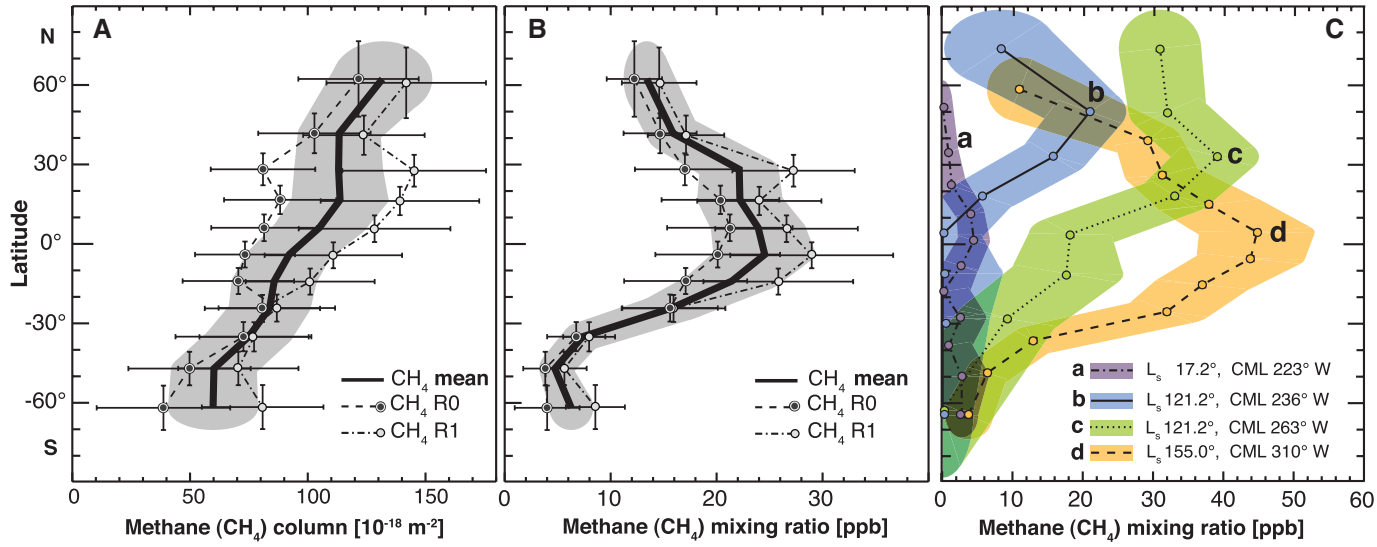


Fig. 2. Absolute abundances, spatial profiles, and seasonal changes of CH_4 on Mars. (**A**) The total CH_4 column density (in molecules per square meter) along a two-way path (Sun to Mars surface and Mars surface to Earth) needed to reproduce the measured lines (after correcting for terrestrial transmittance, SOM-2). The R0 (Fig. 1C) and R1 (Fig. 1B) lines were analyzed independently for a range of longitudes that spanned 46° but differed by 12° in mean longitude (312° for R0 versus 300° for R1, Table 1). The apparent differences in CH_4 column density seen at low latitudes (30°N to 15°S) reflect (in part) differences in mean topography sampled on the two dates. The confidence limits contain both systematic uncertainty and random error; the systematic uncertainty affects all extracted values in the same way whereas the random error introduces scatter among the individual points (SOM-2 and SOM-3). (**B**) The local mixing ratio (in parts per billion) of CH_4 obtained from the column density (A) in each footprint, after correcting for two-way air mass on Mars and for topography (SOM-3). The mixing ratios derived from R0 and R1 of CH_4 agree, within confidence limits. The remaining systematic difference at low latitudes is consistent with stronger weighting of local sources (Fig. 3) on 20 March (R1), when the longitude range sampled was more nearly centered over them. The differences in mixing ratio (R0 versus R1) should then have decreased with increasing distance from the source or sources, as they did (compare values at 60°N, 40°N, and 25°S, 35°S, 47°S, and 62°S). (**C**) Geographic and temporal variability of Mars CH_4. Latitudinal profiles of CH_4 mixing ratios for different longitudes and seasons are shown; the width of the color envelope represents the $\pm 1\sigma$ confidence envelope. The areocentric seasons (L_s) are early northern spring (a: 17°), early northern summer (b and c: 122°), and late northern summer (d: 155°) (Table 1). These extracts are taken from spectra centered at the indicated longitude (CML), and the sub-Earth footprints span longitude-latitude ranges (Table 1) with these physical dimensions: a, 770 km × 535 km; b and c, 1274 km × 818 km; d, 948 km × 586 km. The mixing ratios shown in profile d are larger than those shown in Fig. 2B, owing to different longitudinal binning, and they reflect the longitudinal maximum of the plume (SOM-1, figs. S1 and S6, and Fig. 3).

clear maximum for each north-south spatial profile (Fig. 2C). Moving southward by about 30° from the latitude of the peak, the mixing ratio decreased by a factor of 2 in each case, and for profile d the northward gradient was similar to the southward one. These latitudinal gradients suggest that there was a local source or sources and the resulting plume or plumes were being dispersed by atmospheric circulation.

We consider the dimension of the hypothesized CH_4 plume to be about 60° in latitude [full width at half maximum (FWHM); Fig. 2C, profile d] and assume a similar dimension in longitude. The latter view is weakly supported by profiles b and c, which differ by 27° in central longitude and by a factor of 2 in peak mixing ratio. It is also supported by the profile formed by binning over 46° in longitude (277° to 323°, Fig. 2B), which has a peak mixing ratio [24 parts per billion (ppb)] reduced by a factor of 2 from the peak value (45 ppb) obtained when binning over only 16° of longitude (302° to 318°, Fig. 2C, profile d). The slight increase of profile d near 40° N is consistent with enhanced CH_4 (perhaps owing to continued release at that latitude; compare profiles b and c), whereas the slight increase in profile c near 15°S suggests a small contribution from a source to the west (compare peak position, profile d). Together, these profiles suggest that there may be two local source regions, the first centered near 30°N, 260°W and the second near 0°, 310°W. The vapor plume from each is consistent with ~60° in both latitude and longitude.

The amount of trace gas present in each plume can be estimated from these parameters (SOM-4). In the central plume of profile d (FWHM diameter ~60°), the mean CH_4 mixing ratio is ~33 ppb (120 mol km^{-2}), and the plume contains ~1.17×10^9 mol of CH_4 (~1.86×10^7 kg, or ~19,000 metric tons). If seasonally controlled, the duration of release must be substantially shorter than 0.5 MYs, requiring a mean CH_4 release rate of ≥39 mol s^{-1} (≥0.63 kg s^{-1}). For comparison, the massive hydrocarbon seep field at Coal Oil Point in Santa Barbara, California, releases CH_4 at a rate of ~0.4 to 1.0 kg s^{-1} (*28*).

We considered three models for plume formation, to constrain aspects of CH_4 release and its migration in latitude and longitude (SOM-5). A model based on release from a central source region coupled with eddy diffusion fits the observed plume parameters. Models of meridional flow using a global circulation model suggest that released gas would move northward by ~3.3 cm s^{-1} at this season (*29*), for a total displacement by not more than ~170 km from its central source. If the mixing coefficients (K_x and K_y) in zonal and meridional directions are identical (K_h), a steady source would fill the plume (profile d) in 60 days if $K_h \sim 6.4 \times 10^8$ cm^2 s^{-1}. For this case, the required source strength would be ~3.66 kg s^{-1}. The filling time and K_h vary inversely, whereas K_h and source strength vary proportionately. For a filling time of 0.5 MYs (~344 Earth days), $K_h \sim 1.1 \times 10^8$ cm^2 s^{-1} and the source strength is ~0.63 kg s^{-1}. A reasonable limit for filling time (<120 days) requires $K_h \sim 3.2 \times 10^8$ cm^2 s^{-1} and source strength ~1.8 kg s^{-1}.

These parameters are consistent with release from a single central source region, followed by efficient eddy mixing (SOM-5). The central source could be activated thermally by warming of a surface zone, or by connecting subpermafrost regions to the atmosphere through seasonally opened pores in scarps or crater walls. The plume would reflect the gross morphology of active release zones (and their intensity), and the peak could suggest a region of enhanced release. For comparison, the subsolar latitude was 24°N at L_s = 122° (compare profiles b and c) and 10°N for L_s = 155° (profile d).

Additional information is obtained from a high-resolution map constructed from our data for mid-summer 2003 (Fig. 3 and fig. S1). CH_4 appears notably enriched over several localized areas: A (east of Arabia Terra, where we also measure greatly enriched water vapor), B_1 (Nili Fossae), and B_2 (the southeast quadrant of Syrtis Major). Unusual enrichments in hydrated minerals (phyllosilicates)

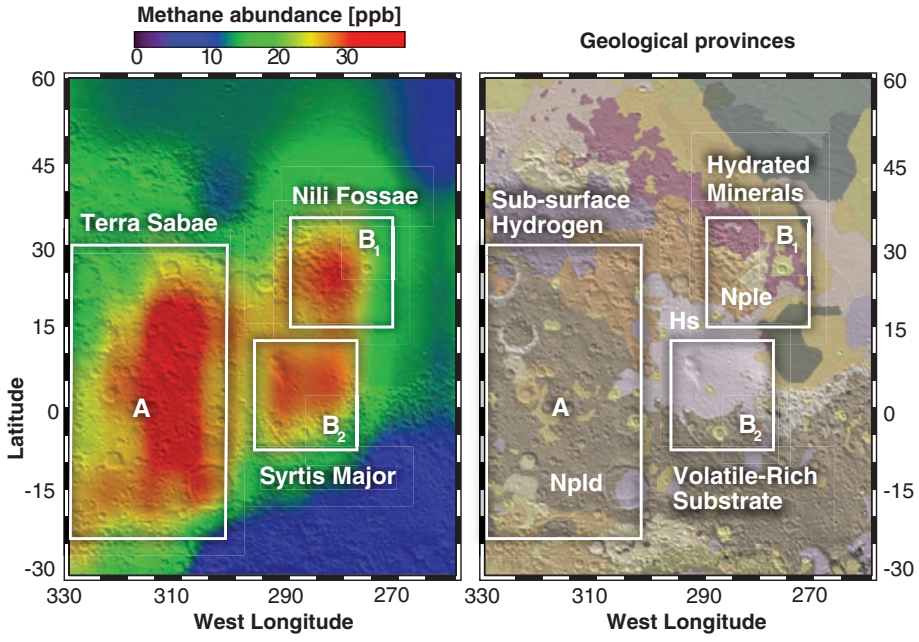


Fig. 3. Regions where CH_4 appears notably localized in northern summer (A, B_1, and B_2) and their relationship to mineralogical and geomorphological domains. (**A**) Observations of CH_4 near the Syrtis Major volcanic district. (**B**) Geologic map of Greeley and Guest (*45*) superimposed on the topographic shaded relief from the Mars Orbiter Laser Altimeter (*46*). The most ancient terrain units are dissected and etched Noachian plains (Npld and Nple) (~3.6 to 4.5 billion years old, when Mars was wet) and are overlain by volcanic deposits from Syrtis Major of Hesperian (Hs) age (~3.1 to 3.6 billion years old).

were identified in Nili Fossae by Mars Express (*30*, *31*) and by the Mars Reconnaissance Orbiter (*32*) (Fig. 3). The observed morphology and mineralogy (*33*, *34*) of this region suggest that these bedrock outcrops, rich in hydrated minerals, might be connecting with reservoirs of buried material rich in volatile species. The characteristic arcuate ridges in the southeast quadrant of Syrtis Major were interpreted as consistent with catastrophic collapse of that quadrant, from interaction with a volatile-rich substrate (*34*).

The low mean abundance measured in early spring 2006 (profile a) provides an important constraint on the CH_4 lifetime. The plume seen in March 2003 (19,000 tons, Fig. 2C, profile d) implies a global mean mixing ratio of ~2 ppb, if later spread uniformly over the planet. The content of the central plume of profile c is similar. Combining data for the entire region mapped during northern summer brings the total CH_4 to 42,000 tons, or 6 ppb if spread uniformly over the planet. However, the mean mixing ratio displayed in the early spring equinox in 2006 (profile a, Fig. 2C) was only 3 ppb (SOM-3). If CH_4 is not removed by other means, the implied destruction lifetime is ~4 Earth years if the 2003 event was singular, to as little as ~0.6 Earth years if the event repeats each MY. In either case, the destruction lifetime for CH_4 is much shorter than the time scale (~350 years) estimated for photochemical destruction (*16*). Another process thus must dominate removal of atmospheric CH_4 on Mars, and it must be more efficient than photochemistry by a factor ≥100.

Heterogeneous (gas-grain) chemistry is a strong candidate. The presence of strong oxidants in the soil was suggested first by the labeled-release experiment on Viking landers, and laboratory simulations suggested that peroxides (such as H_2O_2) were responsible; the apparent discovery of perchlorate ($XClO_4$) by the Phoenix lander (*35*, *36*) suggests the existence of another family of strong oxidants, although their presence at low latitudes has not been established. The lofting of oxidant-coated soil particles into the atmosphere could permit rapid oxidation of the CH_4 that collides with them. H_2O_2 is also produced photochemically and is a known trace gas in the atmosphere (*37*) and (being polar) might bind to aerosol surfaces. Electrochemical processes in dust storms may produce additional peroxide efficiently (*4*, *6*, *23*, *24*) (SOM-6). Peroxide-coated grains might provide an efficient sink for CH_4 for many years thereafter if they settle to the surface and are sequestered in the regolith (*6*, *24*). Sequestered oxidants should also efficiently destroy upward-diffusing CH_4, reducing the fraction that might escape to the atmosphere.

The most compelling question relates to the origin of CH_4 on Mars. The CH_4 we detected is of unknown age—its origin could be ancient (*38*) or perhaps recent. Both geochemical and biological origins have been explored, but no consensus has emerged. Most theses draw on known terrestrial analogs such as production in magma (*19*, *20*) or serpentinization of basalt (*39*), or production by psychrophilic methanogenic biota in Mars-analog cryoregimes such as permafrost (*21*). The annual release of CH_4 from an arctic tundra landscape on Earth (at 72°N) was measured to be 3.15 g m^{-2}, with midsummer CH_4 fluxes of typically 30 mg m^{-2} day^{-1} (*40*). If similar release rates applied to our midsummer plume, the tundra-equivalent area of (assumed uniform) release would be ~6000 km^2 compared with a plume footprint ~9.7×10^6 km^2. If CH_4 release were uniform over the plume footprint, the mean release rate could be smaller than the arctic rate by a factor of ~1600.

Of special interest are the deep biocommunities that reduce sulfate to sulfide using H_2 or abiotic CH_4 as the electron donor, releasing H_2S. These communities thrive at depths of 2 to 3 km in the Witwatersrand Basin of South Africa and have been isolated from the surface (and photosynthesis) for tens of millions of years (*41*, *42*). It might be possible for analogous biota (methanogens or methanotrophs) to survive for eons below the cryosphere boundary on Mars, where water is again liquid, radiolysis can supply energy, and CO_2 can provide a carbon source. Gases accumulated in such zones might be released to the atmosphere if pores or fissures open seasonally, connecting these deep zones to the atmosphere at scarps, crater walls, or canyons. The location of CH_4 maxima over the Syrtis Major shield volcano and the nearby Nili Fossae district suggests a possible relation to serpentinization and/or to the phyllosilicates discovered there (*43*, *44*).

References and Notes

1. H. Nair, M. Allen, A. D. Anbar, Y. L. Yung, R. T. Clancy, *Icarus* **111**, 124 (1994).
2. M. E. Summers, B. J. Lieb, E. Chapman, Y. L. Yung, *Geophys. Res. Lett.* **29**, 2171 (2002).
3. A.-S. Wong, S. K. Atreya, T. Encrenaz, *J. Geophys. Res. Planets* **108**, 7 (2003).
4. S. K. Atreya *et al.*, *Astrobiology* **6**, 439 (2006).
5. R. E. Pellenbarg, M. D. Max, S. M. Clifford, *J. Geophys. Res. Planets* **108**, GDS 23-1 (2003).
6. S. K. Atreya, P. R. Mahaffy, A.-S. Wong, *Planet. Space Sci.* **55**, 358 (2007).
7. W. C. Maguire, *Icarus* **32**, 85 (1977).
8. V. A. Krasnopolsky, G. L. Bjoraker, M. J. Mumma, D. E. Jennings, *J. Geophys. Res.* **102**, 6525 (1997).
9. M. Lellouch *et al.*, *Planet. Space Sci.* **48**, 1393 (2000).
10. M. J. Mumma *et al.*, *Bull. Am. Astron. Soc.* **35**, 937 (2003).
11. M. J. Mumma *et al.*, *Bull. Am. Astron. Soc.* **36**, 1127 (2004).
12. M. J. Mumma *et al.*, *Bull. Am. Astron. Soc.* **37**, 669 (2005).
13. M. J. Mumma *et al.*, *Bull. Am. Astron. Soc.* **39**, 471 (2007).
14. M. J. Mumma *et al.*, *Bull. Am. Astron. Soc.* **40**, 396 (2008).
15. V. Formisano, S. Atreya, T. Encrenaz, N. Ignatiev, M. Giuranna, *Science* **306**, 1758 (2004).
16. V. A. Krasnopolsky, J. P. Maillard, T. C. Owen, *Icarus* **172**, 537 (2004).
17. V. A. Krasnopolsky, *Icarus* **190**, 93 (2007).
18. A. Geminale, V. Formisano, M. Giuranna, *Planet. Space Sci.* **56**, 1194 (2008).
19. J. R. Lyons, C. E. Manning, C. E. Nimmo, *Geophys. Res. Lett.* **32**, L13201 (2005).
20. C. Oze, M. Sharma, *Geophys. Res. Lett.* **32**, L10203 (2005).
21. T. C. Onstott *et al.*, *Astrobiology* **6**, 377 (2006).
22. V. A. Krasnopolsky, *Icarus* **180**, 359 (2006).
23. W. M. Farrell, G. T. Delory, S. K. Atreya, *Geophys. Res. Lett.* **33**, L21203 (2006).
24. G. T. Delory *et al.*, *Astrobiology* **6**, 451 (2006).
25. V. Formisano *et al.*, *Planet. Space Sci.* **53**, 1043 (2005).
26. G. L. Villanueva, M. J. Mumma, R. E. Novak, T. Hewagama, *Icarus* **195**, 34 (2008).

27. We binned spectra over 46° of longitude (centered at CML 300°) for Fig. 1, B and C (and Fig. 2, A and B), but over only 16° for Fig. 2C. Profile d is centered at CML 310°, leading to lower mean mixing ratios in Fig. 2B as compared with Fig. 2C (profile d). See detailed map in Fig. 3.
28. S. Mau *et al.*, *Geophys. Res. Lett.* **34**, L22603 (2007).
29. M. A. Mischna, M. I. Richardson, R. J. Wilson, D. J. McCleese, *J. Geophys. Res.* **108**, 5062 (2003).
30. F. Poulet *et al.*, *Nature* **438**, 623 (2005).
31. J. P. Bibring *et al.*, *Science* **312**, 400 (2006).
32. J. F. Mustard *et al.*, *Nature* **454**, 305 (2008).
33. H. Hiesinger, J. W. Head III, *J. Geophys. Res.* **109**, E01004 (2004).
34. D. Baratoux *et al.*, *J. Geophys. Res.* **112**, E08S05 (2007).
35. M. H. Hecht *et al.*, *Eos* **89**, *Fall Meeting Suppl.*, U14A-04 (abstr.) (2008).
36. S. P. Kounaves *et al.*, *Eos* **89**, *Fall Meeting Suppl.*, U14A-05 (abstr.) (2008).
37. T. Encrenaz *et al.*, *Icarus* **195**, 547 (2008).
38. M. D. Max, S. M. Clifford, *J. Geophys. Res.* **105**, 4165 (2000).
39. D. S. Kelley *et al.*, *Science* **307**, 1428 (2005).
40. C. Wille, L. Kutzbach, T. Sachs, D. Wagner, E.-M. Pfeiffer, *Glob. Change Biol.* **14**, 1395 (2008).
41. T. C. Onstott *et al.*, *Geomicrobiol. J.* **23**, 369 (2006).
42. L.-H. Lin *et al.*, *Science* **314**, 479 (2006).
43. J.-P. Bibring *et al.*, *Science* **312**, 400 (2006).
44. J. F. Mustard *et al.*, *Nature* **454**, 305 (2008).
45. R. Greeley, J. E. Guest, *U.S. Geol. Surv. Map I-1802-B* (1987).
46. D. E. Smith *et al.*, *J. Geophys. Res.* **106**, 23689 (2001).
47. We thank T. C. Onstott and L. M. Pratt for helpful comments and two anonymous referees for their comments and suggestions. This work was supported by NASA [the Planetary Astronomy Program (RTOP 344-32-07 to M.J.M), Astrobiology Institute (RTOP 344-53-51, to M.J.M), and Postdoctoral Program (G.L.V.)] and by NSF (Research at Undergraduate Institutions Program AST-0505765 to R.E.N.). We thank the director and staff of NASA's InfraRed Telescope Facility (operated for NASA by the University of Hawaii) for exceptional support throughout our long Mars observing program. Data were also obtained at the W. M. Keck Observatory, operated as a scientific partnership by CalTech, the University of California Los Angeles, and NASA.

Supporting Online Material

www.sciencemag.org/cgi/content/full/1165243/DC1
SOM Text
Figs. S1 to S6
References and Notes

28 August 2008; accepted 6 January 2009
Published online 15 January 2009;
10.1126/science.1165243
Include this information when citing this paper.

Isotopic Evidence for an Aerobic Nitrogen Cycle in the Latest Archean

Jessica Garvin,[1] Roger Buick,[1]* Ariel D. Anbar,[2,3] Gail L. Arnold,[2] Alan J. Kaufman[4]

The nitrogen cycle provides essential nutrients to the biosphere, but its antiquity in modern form is unclear. In a drill core though homogeneous organic-rich shale in the 2.5-billion-year-old Mount McRae Shale, Australia, nitrogen isotope values vary from +1.0 to +7.5 per mil (‰) and back to +2.5‰ over ~30 meters. These changes evidently record a transient departure from a largely anaerobic to an aerobic nitrogen cycle complete with nitrification and denitrification. Complementary molybdenum abundance and sulfur isotopic values suggest that nitrification occurred in response to a small increase in surface-ocean oxygenation. These data imply that nitrifying and denitrifying microbes had already evolved by the late Archean and were present before oxygen first began to accumulate in the atmosphere.

All living organisms require fixed nitrogen for the synthesis of vital biomolecules, such as proteins and nucleic acids. Under low-oxygen conditions, nitrogen-fixing organisms meet this need by reducing dinitrogen gas (N_2) to ammonium (NH_4^+), which is readily incorporated into organic matter. All other organisms rely upon the degradation of N_2 fixers through ammonification to fulfill their nitrogen requirements. Although the evolved NH_4^+ is stable under anoxic conditions, the presence of O_2 in the surface ocean promotes nitrification, the microbial oxidation of NH_4^+ to nitrite (NO_2^-) or nitrate (NO_3^-). These oxidized species are either assimilated by organisms or, under low-oxygen conditions, biologically reduced and ultimately released to the atmosphere. The latter process provides a conduit for loss of fixed N from the ocean and proceeds via denitrification, the stepwise reduction of NO_3^- or NO_2^- to NO, N_2O, and finally N_2, or by anammox, the coupling of NH_4^+ oxidation to NO_2^- reduction. Because unique isotopic fractionations are imparted during many of these transformations, the nitrogen isotopic composition $\delta^{15}N$ (*1*) of organic matter preserved in ancient sediments provides information about the evolution of the N cycle. Here we report $\delta^{15}N$ and total nitrogen (TN) measurements, as well as $\delta^{13}C_{org}$ and total organic carbon (TOC) data, obtained at a resolution of approximately one data point per meter from ~100 m of continuous drill core through the ~2.5–billion-year-old Mount McRae Shale, Hamersley Group, Western Australia (*2*).

If the fixed N reservoir is a steady-state system, the $\delta^{15}N$ of fixed N input and output will be equal ($\delta^{15}N_{input} = \delta^{15}N_{output}$). The isotope effect ε (*3*) imparted during fixed N input is approximated by the difference in $\delta^{15}N$ between the atmospheric N_2 source and the fixed N product ($\varepsilon_{input} = \delta^{15}N_{dinitrogen} - \delta^{15}N_{input}$, where $\delta^{15}N_{dinitrogen} = 0$‰), whereas that of the fixed N output is approximated by the difference in $\delta^{15}N$ between the oceanic fixed N source and the N_2 product ($\varepsilon_{output} = \delta^{15}N_{fixed\ N} - \delta^{15}N_{output}$). Thus, the mean $\delta^{15}N$ of oceanic fixed N is roughly equal to the difference in ε between the output and input processes ($\delta^{15}N_{fixed\ N} = \varepsilon_{output} - \varepsilon_{input}$). In the modern ocean, N_2 fixation is the primary source of fixed N, and denitrification the primary sink. Although fractionation during N_2 fixation is minimal, with $\varepsilon_{N_2\ fixation} = -3$ to +4‰ (*4*, *5*), the isotope effect of denitrification from both NO_3^- and NO_2^- is large, with $\varepsilon_{denitrification} = +20$ to +30‰ (*4*). This results in a residual NO_3^- pool substantially enriched in ^{15}N. Thus, the +5‰ mean isotopic value of modern deep-ocean NO_3^- is attributed to the fractionation imparted during denitrification. Furthermore, because fixed N upwelled to the surface ocean is completely consumed by primary producers under most conditions (*6*), the $\delta^{15}N$ value of organic matter in well-preserved ancient sediments should record the mean $\delta^{15}N$ of oceanic fixed N.

The organic-rich Mount McRae Shale was deposited at 2.5 billion years ago (Ga), shortly before the main rise in O_2 2.45 to 2.22 Ga (*7*). Its geological setting, the sampling procedure, and analytical methods are described in the Supporting Online Material. In the lower portion of the sampled section (Fig. 1), $\delta^{15}N$ values average around +2.5‰ with relatively little variation (+1.3 to +3.8‰). They rise from +1.0‰ at ~161 m to a peak of +7.5‰ at 139 m, then fall back to +2.5‰. The rise in $\delta^{15}N$ roughly correlates with an enrichment in TOC between 153 and 126 m, from 3 to 16 weight percent (wt %). Additionally, atomic C/N ratios increase from ~150 to ~65 from base to top. $\delta^{13}C_{org}$ values vary little below 150 m, consistently falling between –36 and –42‰. There is no $\delta^{13}C_{org}$ excursion corresponding to the $\delta^{15}N$ spike. Instead, $\delta^{13}C_{org}$ values rise from –42 to –34‰ above 134 m, corresponding to a decrease in $\delta^{15}N$ values.

Given the low metamorphic grade (prehnite-pumpellyite facies to < 300°C) of the Mount McRae Shale (*8*), preferential $^{14}NH_4^+$ loss during high-temperature devolatilization should not have greatly affected $\delta^{15}N$ preservation (*9*). The direct relation between TN and $\delta^{15}N$ (Fig. 1) further supports minimal metamorphic $\delta^{15}N$ alteration because $^{14}NH_4^+$ loss would produce the opposite relation. The relatively high C/N ratios are typical of Precambrian organic matter (*10*) and reflect preferential degradation of organic N during diagenesis. The C/N decrease upsection may result from increased adsorption of diagenetically produced NH_4^+ onto clay minerals or its substitution for K^+ in K-bearing minerals. If so, the lack of covariation between $\delta^{15}N$ values and C/N ratios implies that diagenetic $\delta^{15}N$ alteration was

[1]Department of Earth and Space Sciences and Astrobiology Program, University of Washington, Seattle, WA 98195–1310, USA. [2]School of Earth and Space Exploration, Arizona State University, Tempe, AZ 85287, USA. [3]Department of Chemistry and Biochemistry, Arizona State University, Tempe, AZ 85287, USA. [4]Department of Geology, University of Maryland, College Park, MD 20742, USA.

*To whom correspondence should be addressed. E-mail: buick@ess.washington.edu